

Finite fracture mechanics predictions on the apparent fracture toughness of as-quenched Charpy V-type AISI 4340 steel specimens

Original

Finite fracture mechanics predictions on the apparent fracture toughness of as-quenched Charpy V-type AISI 4340 steel specimens / Sapora, ALBERTO GIUSEPPE; Firrao, Donato. - In: FATIGUE & FRACTURE OF ENGINEERING MATERIALS & STRUCTURES. - ISSN 8756-758X. - 40:6(2017), pp. 949-958. [10.1111/ffe.12555]

Availability:

This version is available at: 11583/2673172 since: 2020-04-24T11:27:01Z

Publisher:

Blackwell Publishing Ltd

Published

DOI:10.1111/ffe.12555

Terms of use:

This article is made available under terms and conditions as specified in the corresponding bibliographic description in the repository

Publisher copyright

(Article begins on next page)

Finite fracture mechanics predictions on the apparent fracture toughness of as-quenched Charpy V-type AISI 4340 steel specimens

Q1 A SAPORA¹ and D FIRRAO²

¹Department of Structural, Geotechnical and Building Engineering, Politecnico di Torino, Corso Duca degli Abruzzi 24 10129 Turin, Italy, ²Department of Applied Science and Technology, Politecnico di Torino, Corso Duca degli Abruzzi 24 10129 Turin, Italy

Received Date: 27 July 2016; Accepted Date: 25 October 2016; Published Online:

ABSTRACT Quenching AISI 4340 steel from 1200 °C leads to much higher fracture toughness in the as-quenched state than by conventional austenitizing at 870 °C. However, the increase is limited to fracture toughness tests, because Charpy V impact/slow bend tests do not show any betterment due to high-temperature austenitizing. Different explanations of these contradicting results have been proposed since the beginning of the 1970s. In the present paper, this puzzling phenomenon will be revisited through the coupled stress and energy criterion in the framework of finite fracture mechanics. The approach involves two material parameters, namely the tensile strength and the fracture toughness, and a critical distance (or finite crack advance), which results to be a structural property. The connection between the critical distance, the microstructure characteristic (i.e. the grain size) and the effective radius involved by other models proposed in the past will be outlined, providing an interesting overview on the studies carried out during the last four decades.

Keywords austenitic grain size; critical distance; CTA steel; FFM; HTA steel; notch radius.

NOMENCLATURE

- d_g =average grain size
- K_I =stress intensity factor
- K_{Ic} =fracture toughness
- K_I^U =apparent stress intensity factor
- K_{Ic}^U =apparent fracture toughness
- l_c =critical crack advance
- ρ =notch root radius
- ρ_{eff} =effective radius
- σ_0 =fitted strength
- σ_f =microstructural critical stress
- σ_u =tensile strength
- σ_y =tensile stress ahead of the notch tip
- σ_Y =yield strength

INTRODUCTION

High-temperature austenitizing (HTA) of steels, that is, austenitizing at temperatures well above the A_{c3} critical point, has been historically considered detrimental because it promotes large austenitic grain growth and, in turn, the raise of the ductile-to-brittle transition temperature, as measured by Charpy V-type specimens, with respect to conventionally austenitized (CTA) steels. Around 1969 in

the then USSR and 1972 in the USA, a scientific movement towards the adoption of HTA was born, based on a spectacular raise of fracture toughness of as-quenched low-alloy high-strength steels upon increasing the austenitizing temperature.^{1,2} On the other hand, Charpy V impact tests still confirmed that austenitization at the usual ($A_{c3} + 50$ °C) temperature yielded larger absorbed energy values than by adopting HTA.^{3–5} The previously described contradictory phenomenon of the different influence of HTA and CTA on fracture properties of precracked and round notch samples was further confirmed by slow bend tests⁶ on

Correspondence: A. Sapora. E-mail: alberto.sapora@polito.it

as-quenched AISI 4340 steel Charpy V-type bars with varying notch root radii ρ , austenitized at low and high temperatures and quenched in oil.

By mid-1980s, HTA was abandoned on the assumption that no industrial application could be associated with it. Nowadays, lightweight design calls for the use of high-strength fasteners with tensile strengths well above those foreseen by the 12.9 property class (ISO 898-1 standard). Whereas the requirement has opened again explorations into high-strength low-alloy steels quenched and tempered at low temperatures, the adoption of HTA might be useful revisiting.

The aim of the present paper is to provide a complete revisitation of the behaviour of HTA and CTA notched steel structures by advancing a micromechanic interpretation of the failure mechanism and by estimating the apparent fracture toughness as a function of the notch radius through the coupled criterion of finite fracture mechanics (FFM).⁷ The approach considers as a necessary and sufficient condition for fracture to propagate in a brittle way the contemporaneous fulfilment of two conditions: (i) The average locally applied tensile stress must be higher than the material tensile strength σ_u over a finite distance l_c from the notch root and (ii) the energy available by crack propagation over l_c must be greater than the fracture energy, which is a function of the fracture toughness K_{Ic} by means of Irwin's relationship. The distance l_c results to be a structural parameter, depending both on the material properties σ_u and K_{Ic} and on the geometry (i.e. the root radius ρ for what concerns blunt-notched structures under mode I loading conditions). A similar approach, but based on a punctual stress condition, was developed by Leguillon.⁸ The coupled criteria have been generally referred to as FFM in recent studies, distinguishing somehow them from those based just either on a stress requirement or on an energy condition, according to which l_c is a material constant. Indeed, all the (coupled or not) approaches belong to the wider framework of the theory of critical distances.⁹

Finite fracture mechanics has been successfully applied to elements containing different features (such as holes, cracks, V-notches, interfaces) subjected to different loading conditions (from mode I to mode II and mixed mode), and the experimental verification has generally involved ceramic or polymeric materials, such as poly (methyl methacrylate) or polystyrene.^{10–14} On the other hand, for what concerns metallic materials, no studies seem to have been performed so far, apart from those carried out through the simple point stress and average stress criteria,^{9,15} a preliminary attempt by Sapora *et al.*¹⁶ (see also Firrao *et al.*¹⁷), and the recent analysis on fatigue strength by means of the strain energy density criterion.^{18,19}

Finally, it has to be observed that both the stress field function²⁰ and the stress intensity factor (SIF) function²¹

providing the crack driving force are available in the literature, thus allowing a semi-analytical approach.

EXPERIMENTAL PART

To enlarge the range of experimental data on which to apply the previously described FFM coupled criteria and to further investigate into the role of the purity of steels and of the prior austenitic grain size, Charpy V-type sharp crack as well as blunt notch samples from two more different heats of AISI 4340 steels were fabricated, in addition to previously tested samples.⁶ Varying notch root radii ρ up to 1.6 mm having been machined, new specimens were slow bend tested in the as-quenched condition, both from HTA or CTA. Thus, alongside the heat previously tested (A steel), B and C steel heats, as listed in Table 1, were sampled. A and B steels were fabricated by electric arc furnace, whereas C steel was further vacuum arc remelted to reduce P and S contents. All the steels were received in the hot rolled and annealed condition. Whereas A steel had been received in the form of 50 mm square bar,⁵ B and C steels were in the form of cylindrical bars, 70 and 85 mm dia., respectively. Notches and fatigue precracks having been machined in the longitudinal-transverse directions for A steel, they were obtained in the LR direction for B and C steel. Also, tensile specimens in the longitudinal direction were fabricated and heat treated.

Although A and B steels have a very similar composition, the inclusion type and distribution were quite different; in A steel, it was possible to recognize only elongated sulphides, whereas in B steel, thin sulphides were accompanied by a few large round inclusions, identified as silicon aluminates. C steel had a very limited amount of slightly elongated sulphides and widely spaced round inclusions.

As before,^{5,6} HTA was performed by austenitizing 1 h at 1200 °C with subsequent cooling to 870 °C for 0.5 h prior to oil quench to minimize distortions and to avoid quench cracks at the root of the notch if a direct quench from the high temperature had been used. CTA foresaw 1 h austenitizing at 870 °C and oil quench. The whole heat-treating procedure was performed in salt baths, carefully controlled for neutrality. ASTM E399 and

Table 1 Chemical composition of sampled heats of AISI 4340 steel (wt pct)

Steel	C	Mn	Ni	Cr	Mo	Si	P	S
A	0.40	0.75	1.74	0.81	0.23	0.26	0.019	0.015
B	0.41	0.75	1.69	0.78	0.24	0.27	0.016	0.015
C	0.41	0.82	1.80	0.85	0.26	0.22	0.009	0.003

E8/E8M standards were adopted for fracture toughness and tension testing by an MTS 250 kN servo-hydraulic testing system. Tensile test results are reported in Table 2.

For all the steels, HTA resulted in lower values of the tensile strength σ_u and elongation to fracture with respect to CTA and in a negligible (A and B steels) or small variation (C steel) of the yield strength σ_Y .

Also, in the case of B and C steels, as for A steel,⁶ load deflection diagrams during fracture toughness testing were essentially linear up to instability with almost nil subcritical crack growths for all the samples. Thus, fracture toughness K_{Ic} values computed at maximum load could be employed to obtain critical applied \mathcal{J}_c integral values by the relationship $\mathcal{J}_c = (1 - \nu^2)K_{Ic}^2/E$. Collective fracture toughness results have been recently published in such a form by the authors.¹⁷ Blunt notch apparent fracture toughness results lay predominantly on sloped straight lines passing through the origin in the \mathcal{J} - ρ diagrams either for HTA or CTA specimens. All the HTA sloped lines superimpose, whichever is the steel, and show a lower slope than the corresponding CTA ones. CTA C steel results lay on a much higher slope straight line than for A and B steels, showing that the absorbed fracture energy is higher in that case.

Fracture toughness results and FFM applications are presented and discussed here.

FRACTURE MODES OF HIGH-TEMPERATURE AUSTENITIZING AND CONVENTIONAL TEMPERATURE AUSTENITIZING STEEL SAMPLES

Previous results⁶ show that both A steel HTA and CTA K_{Ic} (sharp crack) specimens failed by brittle intergranular mode. Different fracture morphologies were instead encountered whilst examining rupture surfaces of round V-notch samples. All the HTA samples failed by a predominantly brittle intergranular fracture, irrespective of the ρ value. Instead, CTA samples with a sufficiently large ρ showed a peculiar fracture path with the formation of a continuous shear lip emanating at some distance

Table 2 Tensile properties of the steels in the as-quenched condition from CTA or HTA

Steel	σ_Y (MPa)	σ_u (MPa)	Elongation to fracture (%)
A (CTA)	1695	2060	5.2
A (HTA)	1715	1980	3.2
B (CTA)	1710	2110	7.5
B (HTA)	1705	1930	4.2
C (CTA)	1820	2235	6.8
C (HTA)	1740	1965	3.0

from the notch centreline and then travelling along a logarithmic spiral to the region of the sample minimum section²² (Fig. 1). Larger and larger shear lips were detected as the ρ value increased. These features were associated with a slip line field forming at the root of the notch under the applied slow bending loads. Critical \mathcal{J} integral values at increasing ρ s were found in direct correspondence with the length of the arc of slip lines travelled by the crack during the plastic instability prior to final fracture along the sample centreline. Similar behaviours were detected in round notch samples fabricated with other types of alloy steels with low strain hardening exponents.²³

A quite similar behaviour was ascertained in the case of B and C steel samples, with brittle intergranular morphologies covering all HTA samples and sharp crack CTA specimen fracture surfaces. Also, fractured blunt notch CTA samples showed ductile transgranular features with few areas of quasi cleavage as in the case of A steel. The characteristic feature represented by the initial propagation along logarithmic spirals replicates also for B and C steel blunt notch samples, with the only difference being that in the case of C steel specimens, fracture initiation tends to be further apart from the notch centreline than for similar A and B steel samples. Because \mathcal{J} values for C steel are higher than corresponding values for A and B steels at the same ρ , it means that in the C steel case, its larger cleanness promotes larger plastically deformed volumes at the root of the notch, as demonstrated previously.²³

FINITE FRACTURE MECHANICS APPROACH

Let us refer to the coordinate system for a U-notch geometry displayed in Fig. 2. The coupled FFM criterion for mode I loading conditions can be formulated as¹¹:

$$\begin{cases} \int_0^{l_c} \sigma_y(x) dx = \sigma_u l_c \\ \int_0^{l_c} K_I^2(a) da = K_{Ic}^2 l_c \end{cases} \quad (1)$$

It represents a system of two equations in two unknowns: the critical crack extension, l_c , and the failure load, implicitly embedded in the functions for both the stress field $\sigma_y(x)$ and the SIF $K_I(a)$ related to a crack of length a stemming from the notch root (Fig. 2).

By assuming that the notch tip radius ρ is sufficiently small with respect to the notch depth, the stress field along the notch bisector could be approximated by means of Creager-Paris' expression²⁰ ($x < \rho/2$):

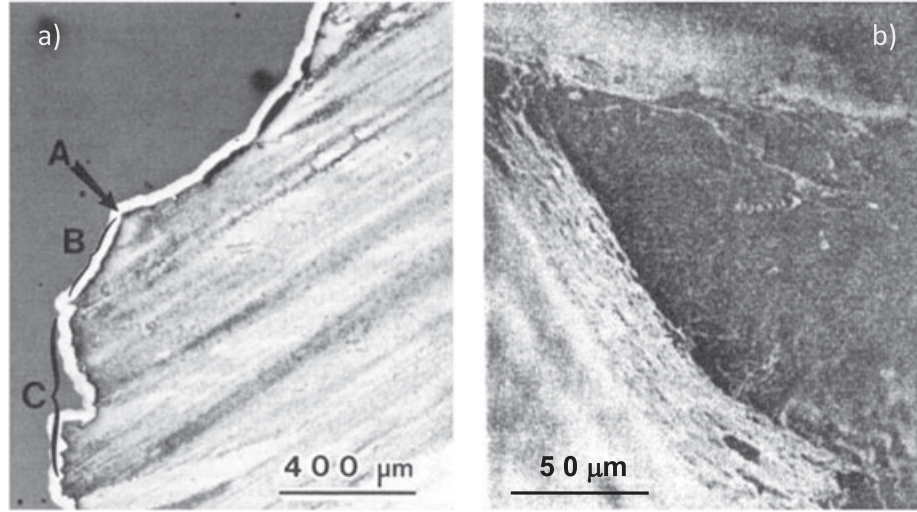


Fig. 1 (a) Fracture path in as-quenched notched specimens austenitized at 870 °C (polished cross section after coating)⁶: initiation (A), propagation along a slip surface (B) and final fracture along the minimum section region (C). (b) Logarithmic spiral along which fracture propagates during B stage.

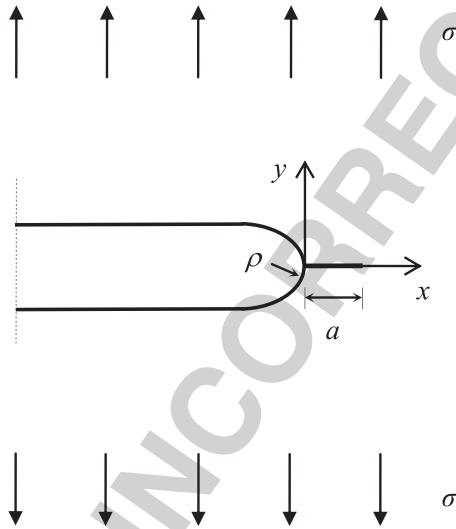


Fig. 2 U-notch geometry with a crack of length a stemming from the notch root.

$$\sigma_y(x) = \frac{2K_I^U}{\sqrt{\pi}} \frac{x + \rho}{(2x + \rho)^{3/2}} \quad (2)$$

where K_I^U is the apparent SIF.²⁴

On the other hand, let us consider a crack of length a stemming from the notch root (Fig. 2). As far as a is sufficiently small with respect to the notch depth, an analytical function for the SIF function was proposed by Sapora *et al.*²¹ in the more general context of blunt V-notches. The expression fulfils the asymptotic limits of very short and very long (but still small with respect

to the notch depth) cracks, providing errors below 1% over the range $0 \leq a/\rho \leq 10$. By setting the notch amplitude equal to 0° as in the present U-notch case, we have:

$$K_I(a) = \left\{ 1 + \left[\frac{\rho}{5.02a} \right]^{1.82} \right\}^{-0.275} K_I^U \quad (3)$$

An alternative expression to (3) was presented by Lukas²⁵ dealing with an elliptical hole and providing a 5% error when used to simulate a crack, that is, when the minor axis to major axis length ratio of the ellipse tends to zero. For other past models, see also the works by Schijve²⁶ and by Xu *et al.*²⁷

Inserting Eqs. (2) and (3) into system (1) and integrating, some analytical manipulations yield:

$$\begin{cases} K_{Ic}^U = f(l_c) \sqrt{\rho} \sigma_u \\ K_{Ic}^U = \sqrt{b(l_c)} K_{Ic} \end{cases} \quad (4)$$

where

$$f(l_c) = \sqrt{\pi(1 + 2l_c/\rho)}/2 \quad (5)$$

and

$$b(l_c) = \frac{l_c}{\int_0^{l_c} \left[1 + \left(\frac{\rho}{5.02a} \right)^{1.82} \right]^{-0.549} da} \quad (6)$$

In the limit case of a sharp crack ($\rho \rightarrow 0$), the energy balance in (4) provides $K_I = K_{Ic}$, and FFM predictions thus

equal those by linear elastic fracture mechanics. The stress condition gives $l_c = 2/\pi \cdot (K_{Ic}/\sigma_u)^2$, which coincides with the distance set by the average stress approach.²⁸ On the other hand, for a smooth element ($\rho \rightarrow \infty$), the failure condition $\sigma = \sigma_u$ follows from the stress requirement, whereas the energy condition provides $l_c = 2/(\pi \cdot 1.122^2) \cdot (K_{Ic}/\sigma_u)^2$, that is, the crack advance according to quantized fracture mechanics.^{29,30}

System (4) can be eventually rearranged in the following form:

$$\begin{cases} \sqrt{\rho} = \frac{\sqrt{b(l_c)}K_{Ic}}{f(l_c) \sigma_u} \\ K_{Ic}^U = \sqrt{b(l_c)}K_{Ic} \end{cases} \quad (7)$$

Thus, once the material properties and the radius are known, the first equation in (7) provides the value of the critical distance l_c , which must then be inserted into the second equation of (7) to get the apparent fracture toughness K_{Ic}^U .

Finally, it is important to remind that the coupled FFM approach (as well as most of the criteria based on critical distance) was proposed to deal with materials failing by brittle fracture, that is, by unstable crack propagation above a critical load. Different materials can belong to this 'class', although involving different failure micromechanisms. The validity of the analysis and of the equations presented in this section can be assumed as long as the small-scale yielding assumption is verified. Observe that some approaches^{15,31} in the framework of theory of critical distances have been recently proposed even to predict ductile failure of U-notched structures under large-scale yielding conditions.

FINITE FRACTURE MECHANICS PREDICTIONS AND DISCUSSION OF RESULTS

The coupled FFM criterion expressed by system (7) is now applied to experimental results on CTA and HTA steel samples. Once the geometry is fixed, the values of the material properties need to be known. The estimations of both the tensile strength σ_u and the fracture toughness K_{Ic} obtained experimentally are reported in Tables 2 and 3. Nevertheless, the values of σ_u cannot be implemented directly to get accurate FFM predictions, because they describe the behaviour of plain specimens that, in some CTA conditions, broke by involving a degree of plastic deformations before failure. Note that some plastic deformation was present even in HTA specimens. In the following, σ_u will be thus replaced by σ_0 (Table 3), whose values were fitted to minimize the mean

Table 3 Fracture toughness and fitted FFM strength of the steels in the as-quenched condition from CTA or HTA

Steel	K_{Ic} (MPa m ^{0.5})	σ_0 (MPa)
A (CTA)	43	6500
B (CTA)	43	6300
C (CTA)	42	9000
A (HTA)	74	3100
B (HTA)	54.5	3700
C (HTA)	47.5	4100

squared error between FFM results and experimental data in terms of the apparent fracture toughness K_{Ic}^U .

In the next section, the physical meaning of σ_0 will be investigated by considering the micromechanics of the failure mechanism, but for the moment, σ_0 can be thought as a mere fitting parameter. Note that a similar procedure on σ_0 is generally adopted also for polymers,^{9,16} due to the presence there of microcracks/defects and crazing phenomena affecting the strength of un-notched specimens.

Estimations on σ_0 for HTA microstructures are lower than those for CTA ones, reflecting the fact that HTA-treated tensile specimens showed a lower elongation to fracture. The ratio σ_0/σ_u is comprised in the range of 1.5–2.1 as it concerns HTA steels, whereas it grows up to 3–4 as it regards CTA ones. Interestingly, A and B CTA steels (which present the same inclusion content) show nearly the same value of σ_0 , whereas that of C steel is the highest for both CTA and HTA samples.

Finite fracture mechanics results on the apparent fracture toughness are reported in Figs. 3, 4 and 5 for A steel, B steel and C steel, respectively. As it concerns HTA steels, there is a perfect agreement with experimental data, whereas the accuracy decreases for the largest root

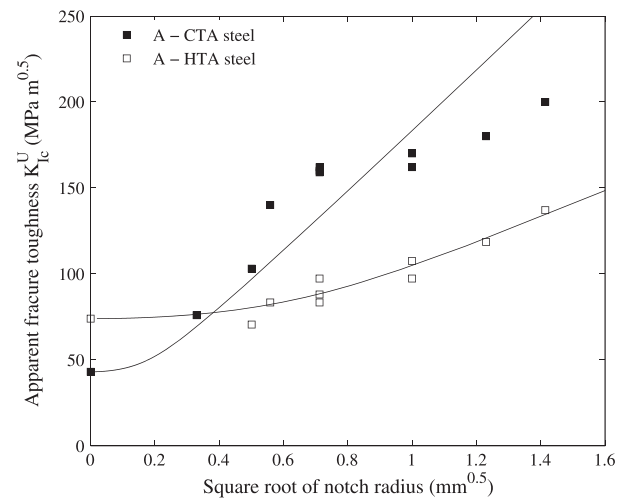


Fig. 3 A steel: FFM predictions carried out on experimental data by Firrao *et al.*⁶

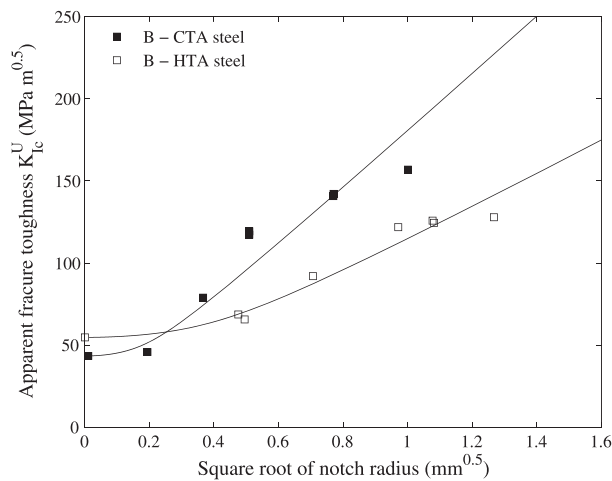


Fig. 4 B steel: FFM predictions carried out on experimental data by Firrao *et al.*²³

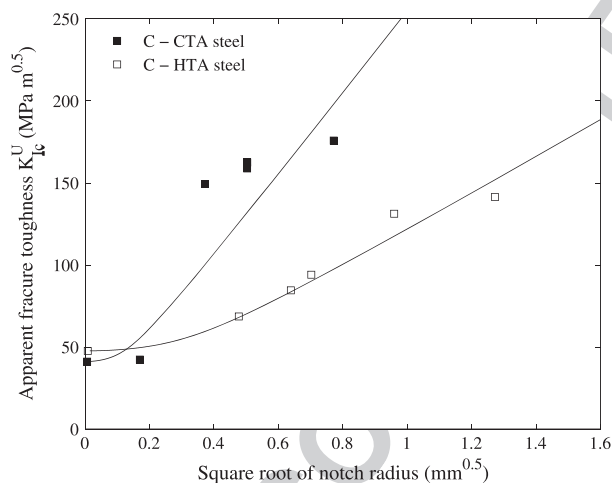


Fig. 5 C steel: FFM predictions carried out on experimental data by Firrao *et al.*²³

radii of CTA steel samples. In this case, the maximum percentage error grows up to nearly 20%, which however can be still considered acceptable. In order to justify the lack of FFM precision as ρ increases for CTA steels, it should be said, first of all, that if the notch radius is not negligible with respect to the notch depth (2 mm for Charpy V-type bars), the asymptotic expressions (3) and (5) can reveal to be inaccurate, resulting in overestimated FFM predictions. Although they may be improved by considering higher order terms in the asymptotic expansions for $\sigma_y(x)$ and $K_I(a)$ (or by carrying out a finite element analysis), this discrepancy is not detected for HTA specimens, which possess the same geometry. Thus, another realistic explanation is that as ρ increases, involving higher failure loads, the level of constraint can reduce as plastic zones become larger.⁹ This phenomenon, as

already described, is more pronounced for CTA structures, where larger shear lips form as ρ increases.

Some comments should be added about the factors that favour the occurrence of shear slip fractures instead of the intergranular ones. Unpublished data obtained by the authors with intermediate grain size (80 μm) samples, step-quenched from 1200 $^{\circ}\text{C}$, seem to indicate that smaller grain sizes allow an easier establishment of active slip systems at the root of a notch. A rationale can then be developed on such a basis: When ρ increases, the plastic zone at the root of the concentration enlarges up to the point that it comprises a few grains, thus allowing the activation of macroscopic plastic instabilities along slip surfaces, which are transparent to microscopic defects (grain boundaries, inclusions, etc.). Conversely, with large grains, around 250 μm , the minimum number of grains necessary to let the slip line field to firmly establish pushes the root radius at which it happens to be too a large size.

It is now interesting to compare the FFM critical crack advance l_c with the austenitic grain size d_g (Table 4). Because l_c is a structural parameter, it depends on both the material properties and the radius.^{16,32} Note that several studies have shown that the length parameters highly depend on the structural configuration,^{33,34} and in some cases, this dependence was assumed *a priori*. On the contrary here, l_c comes as a natural output from FFM system (7), representing one of the two unknowns. Its typical behaviour is reported in Fig. 6 for HTA A steel samples: Interestingly, it attains a minimum between the two limit values described in the previous section and which are reported in Table 4. There is a good correspondence between l_c and d_g as it concerns CTA steels, whilst the critical distance reflects the coarse-grained structures for HTA steels, at least from a qualitative point of view.

MICROMECHANICS INTERPRETATION VIA TETELMAN EQUATIONS

The large increase of K_{Ic} in the HTA state with respect to the CTA one was interpreted by Ritchie *et al.*⁴ by

Table 4 Comparison of prior austenitic grain sizes, FFM characteristic distances and ρ_{eff} values for the three examined steels in the as-quenched condition from CTA or HTA

Steel	d_g (μm)	l_c (μm)	ρ_{eff} (μm)
A (CTA)	20	28–22	15
B (CTA)	34	30–24	34
C (CTA)	18	14–11	25
A (HTA)	250	364–291	230
B (HTA)	215	135–108	144
C (HTA)	200	85.9–68.5	98

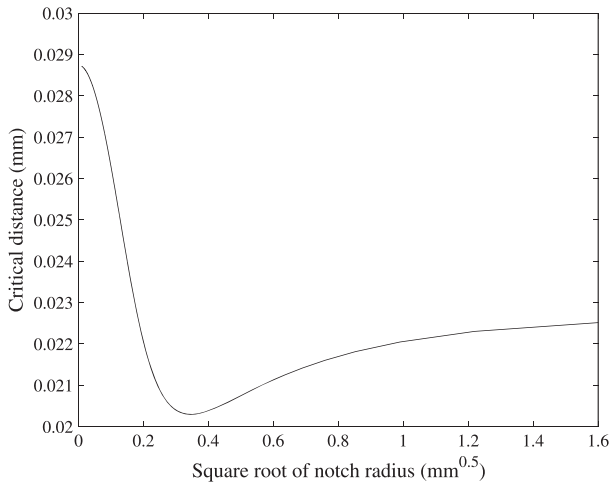


Fig. 6 CTA A steel: FFM critical distance as a function of the notch root radius.

hypothesizing that in the case of small notch specimens failing by brittle intergranular fractures, the controlling parameter is the microstructural characteristic distance, that is, the distance over which the maximum principal stress at the root of the notch, σ_{yy} , has to be larger than the microstructural critical fracture stress, σ_f . The distance is of the same order of magnitude of the steel prior austenitic grain size and coincides with a limiting value of ρ , termed ρ_{eff} . At all values below ρ_{eff} , the apparent fracture toughness is constant and equal to K_{Ic} . The inversion of behaviour between HTA and CTA-notched samples over the notch root radius range above ρ_{eff} was explained calling for the application of Tetelman equations^{35,36}:

$$\begin{cases} K_{Ic} = 2.9\sigma_Y \{ \exp(\sigma_f/\sigma_Y - 1) - 1 \}^{1/2} \rho_{eff}^{1/2} & \text{for } \rho \leq \rho_{eff} \\ K_{Ic}^U = 2.9\sigma_Y \{ \exp(\sigma_f/\sigma_Y - 1) - 1 \}^{1/2} \rho^{1/2} & \text{for } \rho > \rho_{eff} \end{cases} \quad (8)$$

Equation (8) had been derived by combining the elastic solutions of the stress concentration factors of a notch with the slip line field solutions. In large notch samples, failure intervenes at the plastic–elastic interface, located at a greater distance from the tip than in sharp notch samples. By stating that both types of blunt notch samples with $\rho > \rho_{eff}$, either HTA or CTA, failed by a brittle intergranular manner (neglecting shear lips appearing at the root of the notch), Ritchie and co-workers⁴ used Eq. (8) to justify the previously reported behaviour inversion, implying that σ_f for HTA microstructures was smaller than that of CTA ones, thus yielding a less sloped straight line passing through the origin of the K_{Ic}^U versus $\sqrt{\rho}$ diagram. By inserting their values of ρ_{eff} and K_{Ic} into Eq. (8), σ_f for CTA results 60% higher than that obtainable for HTA.

Similar calculations performed on Firrao's results⁶ yield a difference in the same direction. Thus, the high difference in K_{Ic}^U results, resulting in a 43% increase for CTA samples with respect to HTA ones, could be justified. Yet, precise measurements of σ_f via such an indirect method, are hampered by the uncertainty of the precise value of ρ_{eff} to be inserted into Eq. (8).

Note that a similar problem arises when implementing FFM, dealing with the fitted strength σ_0 . Experimental results on CTA steel samples and theoretical predictions according to Tetelman's equations reported in Ritchie *et al.*⁴ are depicted in Fig. 7. In the same figure, FFM predictions are presented by implementing computations with $\sigma_0 = 7800$ MPa. The matching is more than satisfactory: Observe that no large radii were machined, the maximum being 0.56 mm. In this case, the assumption of neglecting shear lips seems thus reasonable. The critical distance is comprised in the range 14.4–11.5 μm , reflecting once again the same order of magnitude of the prior austenitic grain size (24–32 μm).⁴

It is now interesting to compare the two models, to further investigate the physical meaning of σ_0 . By considering a little higher value for σ_0 , namely $\sigma_0 = 8300$ MPa, it can be seen that Eq. (8) provides the exact asymptotes (for small and large radii, respectively) to the FFM curve (dotted line, Fig. 7). Because the slope of the FFM curve for large radii is exactly equal to $\sqrt{\pi}/2 \cdot \sigma_0$, the strength parameter σ_0 must be necessarily a function of the yield strength σ_Y and of the microstructural critical fracture stress σ_f . In formulae, equating the first equation in (4) to the second expression in (8) with the substitution of σ_u with σ_0 yields:

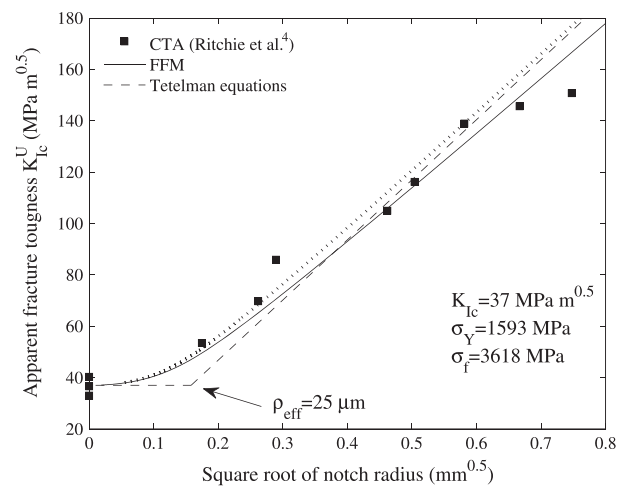


Fig. 7 CTA steel: theoretical predictions according to Tetelman equations (dashed line) and to FFM (continuous line, $\sigma_0 = 7800$ MPa) on experimental data carried out by Ritchie *et al.*⁴ The dotted line refers to FFM results according to $\sigma_0 = 8300$ MPa.

$$\sigma_0 = 3.3\sigma_Y \left\{ \exp(\sigma_f/\sigma_Y - 1) \right\}^{1/2} \quad (9)$$

By looking at the estimations on σ_f deriving from data presented in the literature,^{4,6,17} the following condition is generally satisfied for CTA steel samples: $\sigma_f/\sigma_Y \approx 2.2 - 2.7$. It thus follows from Eq. (9) that $\sigma_0/\sigma_Y \approx 5 - 7$. On the other hand, because usually $\sigma_f/\sigma_Y \approx 1.3 - 1.9$ for HTA microstructures, we have that in such a case $\sigma_0/\sigma_Y \approx 2 - 4$. A good correlation between l_c and ρ_{eff} ¹⁷ is always observed (Table 4), reflecting the fact that the two theories, although derived under different basic assumptions, have some common features.

QUENCHED AND TEMPERED LOW-ALLOY STEELS AUSTENITIZED AT LOW AND HIGH TEMPERATURES

As-quenched low-alloy steels, even austenitized at high temperatures, cannot be used as such in the industrial practice. A temper at least at 200 °C has to be performed to avoid the risk of premature failure in highly stressed components. Zackay *et al.*² had already warned in a workshop that all the beneficial effects upon an increase of fracture toughness by HTA disappeared upon tempering at about 280 °C. For such a reason, two series of eight Charpy V-type blunt notch specimens with varying notch root radii fabricated with A steel were either subjected to CTA or HTA and subsequently tempered at 250 °C. It has to be noted that high-temperature treatment duration was here limited to 40 min to obtain a smaller grain size than before (75 μm) to promote toughness. The experimental mechanical testing procedure was the same one described before. Results indicate that, even by reducing the austenitic grain size to about one-third than before, no large improvement of the HTA blunt notch results can be achieved upon tempering at 250 °C

(Fig. 8).

Finite fracture mechanics predictions obtained by implementing the values for σ_0 reported in Table 5 result again accurate for HTA specimens, l_c reflecting the finer grain size with respect to not tempered steels; an even better correlation exists with ρ_{eff} (110 μm), again signalling the complete adequateness of the FFM approach. On the contrary, the percentage error grows significantly for CTA steel samples with $\rho > 0.57$ mm (Fig. 8), showing that the shear lip mechanism is even more significant than before. Indeed, the elongation to fracture is more than twice of that related to CTA A steel, revealing a more pronounced ductile behaviour. Also here, ρ_{eff} (20 μm) correlates pretty well with l_c .

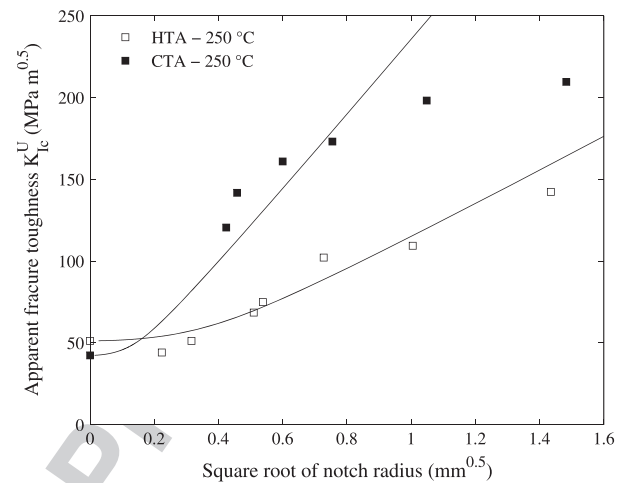


Fig. 8 A steel quenched from HTA and CTA and tempered at +250 °C: FFM predictions on experimental data presented in Firrao *et al.*¹⁷

Table 5 FFM parameters and material properties of AISI 4340 A steel, quenched from CTA and HTA and tempered at 250 °C

Steel	K_{Ic} (MPa m ^{0.5})	σ_0 (MPa)	l_c (μm)	d_g (μm)
CTA +250 °C	42.3	8200	17–13.5	20
HTA +250 °C	51.2	3800	115–92	75

CONCLUSIONS

High-temperature austenitizing at 1200 °C of high-strength low-alloy steels was introduced more than 40 years ago. In the as-quenched state, it offers interesting features; if the austenitic grain size is elevated to about 250 μm from the usual 20 μm size, an almost double increase of the fracture toughness (K_{Ic}) with respect to CTA ensues. Yet, Charpy V-notch absorbed impact energies are lower after HTA than after CTA, as it has long been known. Moreover, HTA-treated tensile specimens show a lower elongation to fracture than CTA ones. Detailed fractographic analysis on AISI 4340 steel slow bend tested specimens, with notch root radii varying from almost nihil to 2 mm, showed that both HTA and CTA sharp notch specimens all failed by brittle intergranular fracture, as well as HTA blunt notch specimens. Instead, CTA blunt notch specimens failed initially by plastic instability along logarithmic spirals of a slip line field emanating at some distance from the notch centreline. The larger the root radius, the larger the slip line.

In the present work, the fracture behaviour of CTA and HTA Charpy V-notch samples has been revisited through the coupled FFM criterion, which is based on a critical distance l_c .

- FFM involves just two material parameters: the fracture toughness K_{Ic} and the tensile strength σ_u . The latter being influenced by large plastic deformations detected during experimental tests, its values were fitted by a parameter termed as σ_0 .
- For approaches similar to the present one, it was claimed that the physical meaning of σ_0 may be questionable.⁹ On the other hand, in the present paper, it was shown that it results from a combination of the yield strength σ_Y and the microstructural fracture stress σ_f invoked by Tetelman's equations. Reliable estimations on σ_0 were furnished for both CTA and HTA steels.
- FFM predictions on HTA steel experiments always reveal to be more than satisfactory, thus confirming the brittle intergranular failure observed during tests.
- FFM predictions on CTA steel experiments result accurate below a limit radius, generally quantified as nearly 0.5–0.6 mm. In the preceding texts, it is not reasonable to neglect the shear lip formation and the subsequent ductility failure mechanism, substantiating the idea that samples break by the achievement of a limiting strain at the notch.
- The length l_c describes significantly the coarse and fine grain size of HTA and CTA AISI 4340 steels either as-quenched or quenched and low temperature tempered and adequately interprets brittle sharp and blunt notch fracture toughness results. Thus, the distance results a structural parameter, which comes as a natural output from FFM system approach.

Eventually, after 40 years of experience with HTA at 1200 °C, it should be added that the treatment still has to be fully explored. Tests on HTA samples, quenched and tempered in the vicinity of 200 °C, are needed to verify that the previously described improvement in fracture toughness over CTA can be, at least partially, maintained to allow useful industrial applications when very high tensile properties are sought.

REFERENCES

- 1 Bashchenko, A. P. and Mel'nichenko, N. D. (1969) Metallovedenie i Term. Obrabot. *Metallov*, **12**, 24–27.
- 2 Zackay, V. F., Parker, E. R., Goolsby, R. D. and Wood, W. E. (1972) Untempered ultra-high strength steels with high fracture toughness. *Nature-Physical Science*, **236**, 108–109.
- 3 Lai, G. Y., Wood, W. E., Clark, R. A., Zackay, V. F. and Parker, E. R. (1974) Effect of austenitizing temperature on microstructure and mechanical properties of as-quenched 4340 steel. *Metall. Trans.*, **5**, 1663–1670.
- 4 Ritchie, R. O., Francis, B. and Server, W. L. (1976) Evaluation of toughness in AISI 4340 steel austenitized at low and high temperature. *Metall. Trans. A*, **7A**, 831–838.
- 5 Roberti, R., Silva, G., De Benedetti, B. and Firrao, D. (1978) Influenza di un trattamento termico di austenitizzazione ad alta temperatura sulle caratteristiche di tenacità di un acciaio AISI 4340 allo stato di piena tempra. *Metall. Ital.*, **70**, 449–475.
- 6 Firrao, D., Begley, J. A., Silva, G., De Benedetti, B. and Roberti, R. (1982) The influence of notch root radius and austenitizing temperature on fracture appearance of as-quenched Charpy-V type AISI 4340 steel specimens. *Metall. Trans. A*, **13A**, 1033–1013.
- 7 Cornetti, P., Pugno, N., Carpinteri, A. and Taylor, D. (2006) Finite fracture mechanics: a coupled stress and energy failure criterion. *Engng Fract Mech*, **73**, 2021–33.
- 8 Leguillon, D. (2002) Strength or toughness? A criterion for crack onset at a notch. *Eur. J. Mech. A/Solids*, **21**, 61–72.
- 9 Taylor, D. (2007) *The Theory of Critical Distances: a New Perspective in Fracture Mechanics*, Elsevier: Oxford, UK.
- 10 Priel, E., Yosibash, Z. and Leguillon, D. (2008) Failure initiation at a blunt V-notch tip under mixed mode loading. *Int J Fract*, **149**, 143–173.
- 11 Carpinteri, A., Cornetti, P., Pugno, N., Sapora, A. and Taylor, D. (2009) Generalized fracture toughness for specimens with re-entrant corners: experiments vs. theoretical predictions. *Struct. Eng. Mech.*, **32**, 609–620.
- 12 Sapora, A., Cornetti, P. and Carpinteri, A. (2013) A finite fracture mechanics approach to V-notched elements subjected to mixed-mode loading. *Eng. Fract. Mech.*, **97**, 216–226.
- 13 Sapora, A., Cornetti, P. and Carpinteri, A. (2014) V-notched elements under mode II loading conditions. *Struct. Eng. Mech.*, **49**, 499–508.
- 14 Weissgraeber, P., Felger, J., Geipel, D. and Becker, W. (2016) Cracks at elliptical holes: stress intensity factor and finite fracture mechanics solution. *Eur. J. Mech. A/Solids*, **55**, 192–198.
- 15 Susmel, L. and Taylor, D. (2008) On the use of the theory of critical distances to predict static failures in ductile metallic materials containing different geometrical features. *Eng. Fract. Mech.*, **75**, 4410–4421.
- 16 Sapora, A., Cornetti, P., Carpinteri, A. and Firrao, D. (2015) An improved finite fracture mechanics approach to blunt V-notch brittle fracture mechanics: experimental verification on ceramic, metallic and plastic materials. *Theor. Appl. Fract. Mec.*, **78**, 20–24.
- 17 Firrao, D., Matteis, P., Cornetti, P. and Sapora, A. (2015) High temperature austenitizing of low alloy steels: what is left after 40 years? In: *28th ASM Heat Treating Society Conference*, Detroit: Michigan, USA, pp. 64–70.
- 18 Gallo, P., Berto, F. and Lazzarin, P. (2015) High temperature fatigue tests of notched specimens made of titanium grade 2. *Theor. Appl. Fract. Mec.*, **76**, 27–34.
- 19 Berto, F., Campagnolo, A. and Lazzarin, P. (2015) Fatigue strength of severely notched specimens made of Ti-6Al-4V under multiaxial loading. *Fatigue Fract. Eng. Mater. Struct.*, **38**, 503–517.
- 20 Creager, M. and Paris, P. C. (1967) Elastic field equations for blunt cracks with reference to stress corrosion cracking. *Int. J. Fract. Mech.*, **3**, 247–252.
- 21 Sapora, A., Cornetti, P. and Carpinteri, A. (2014) Cracks at rounded V-notch tips: an analytical expression for the stress intensity factor. *Int. J. Fract.*, **187**, 285–291.
- 22 Firrao, D., Begley, J. A., De Benedetti, B., Roberti, R. and Silva, G. (1980) Fracture initiation and propagation at the root of the notch of in as-quenched AISI 4340 steel Charpy V-type bars with varying notch root radii. *Scripta Metallurgica*, **14**, 519–524.
- 23 Firrao, D. and Ugues, D. (2005) Fracture of nitrided and nitrocarburized blunt notch three-point bending die steel specimens. *Mater. Sci. Eng. A*, **409**, 309–316.

- 24 Glinka, G. (1985) Energy density approach to calculation of in-elastic strain-stress near notches and cracks. *Engng. Fract. Mech.*, **22**, 485–508.
- 25 Lukas, P. (1987) Stress intensity factor for small notch-emanated cracks. *Eng. Fract. Mech.*, **26**, 471–473.
- 26 Schijve, J. (1982) The stress intensity factor of small cracks at notches. *Fatigue Fract. Eng. Mater. Struct.*, **5**, 77–90.
- 27 Xu, R. X., Thompson, J. C. and Topper, T. H. (1995) Practical stress expressions for stress concentration regions. *Fatigue Fract. Eng. Mater. Struct.*, **22**, 885–895.
- 28 Seweryn, A. (1994) Brittle fracture criterion for structures with sharp notches. *Engng. Fract. Mech.*, **47**, 673–81.
- 29 Pugno, N. and Ruoff, N. (2004) Quantized fracture mechanics. *Philos. Mag. A*, **84**, 2829–45.
- 30 Taylor, D., Cornetti, P. and Pugno, N. (2005) The fracture mechanics of finite crack extension. *Engng. Fract. Mech.*, **72**, 1021–38.
- 31 Torabi, A. R., Habibi, R. and Mohammad Hosseini, B. (2015) On the ability of the equivalent material concept in predicting ductile failure of u-notches under moderate- and large-scale yielding conditions. *Phys. Mesomech.*, **18**, 337–347.
- 32 Carpinteri, A., Cornetti, P. and Sapora, A. (2012) A finite fracture mechanics approach to the asymptotic behavior of U-notched structures. *Fatigue Fract. Eng. Mater. Struct.*, **35**, 451–457.
- 33 Srivastava, V. (2002) Notched strength prediction of laminated composite under tensile loading. *Mater. Sci. Eng. A*, **32**, 302–309.
- 34 Camanho, P. P. and Lambert, M. (2006) A design methodology for mechanically fastened joints in laminated composite materials. *Compos. Sci. Technol.*, **66**, 3004–3020.
- 35 Wilshaw, T. R., Rau, C. A. and Tetelman, A. S. (1968) A general model to predict the elastic-plastic stress distribution and fracture strength of notched bars in plane strain bending. *Engng. Fract. Mech.*, **1**, 191–211.
- 36 Alkin, J. M. and Tetelman, A. S. (1971) Relation between K_{Ic} and microscopic strength for low alloy steels. *Engng. Fract. Mech.*, **3**, 151–67.

Author Query Form

Journal: Fatigue & Fracture of Engineering Materials & Structures






Article: ffe_12555

Dear Author,

During the copyediting of your paper, the following queries arose. Please respond to these by annotating your proofs with the necessary changes/additions.

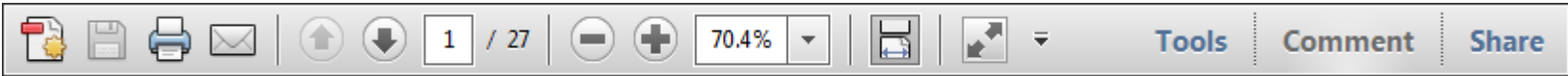
- If you intend to annotate your proof electronically, please refer to the E-annotation guidelines.
- If you intend to annotate your proof by means of hard-copy mark-up, please use the standard proofing marks. If manually writing corrections on your proof and returning it by fax, do not write too close to the edge of the paper. Please remember that illegible mark-ups may delay publication.

Whether you opt for hard-copy or electronic annotation of your proofs, we recommend that you provide additional clarification of answers to queries by entering your answers on the query sheet, in addition to the text mark-up.

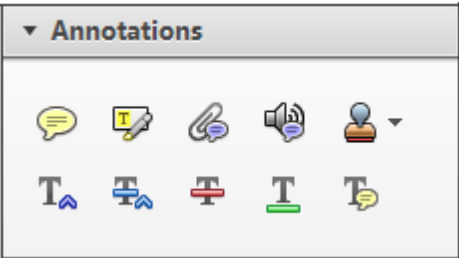
Query No.	Query	Remark
Q1	AUTHOR: Please confirm that given names (red) and surnames/family names (green) have been identified correctly.	
Q2	AUTHOR: "Poly(methyl methacrylate)" was provided as the definition of "PMMA." Please check and change as necessary.	
Q3	AUTHOR: "Long-transverse" was provided as the definition of "LT." Please check and change as necessary.	
Q4	AUTHOR: If "LR" was used as an abbreviation, please provide its definition instead.	
Q5	AUTHOR: If "ASTM" was provided as an abbreviation, please provide its definition instead.	

Required software to e-Annotate PDFs: Adobe Acrobat Professional or Adobe Reader (version 7.0 or above). (Note that this document uses screenshots from Adobe Reader X)
The latest version of Acrobat Reader can be downloaded for free at: <http://get.adobe.com/uk/reader/>

Once you have Acrobat Reader open on your computer, click on the [Comment](#) tab at the right of the toolbar:



This will open up a panel down the right side of the document. The majority of tools you will use for annotating your proof will be in the [Annotations](#) section, pictured opposite. We've picked out some of these tools below:



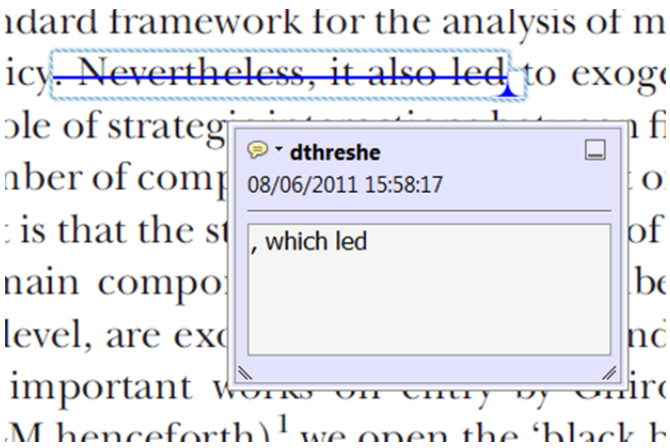
1. [Replace \(Ins\)](#) Tool – for replacing text.



Strikes a line through text and opens up a text box where replacement text can be entered.

How to use it

- Highlight a word or sentence.
- Click on the [Replace \(Ins\)](#) icon in the Annotations section.
- Type the replacement text into the blue box that appears.



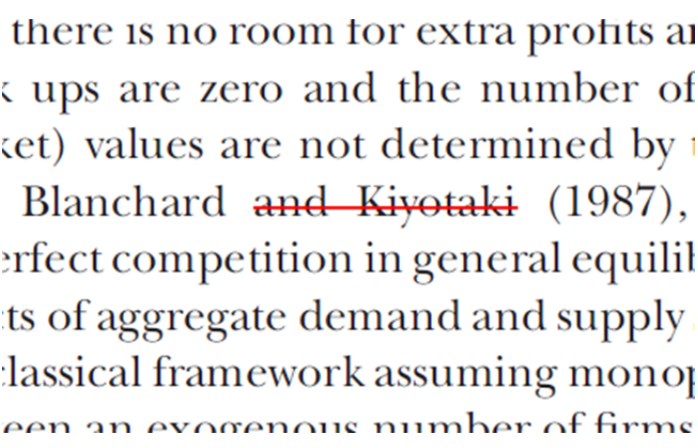
2. [Strikethrough \(Del\)](#) Tool – for deleting text.



Strikes a red line through text that is to be deleted.

How to use it

- Highlight a word or sentence.
- Click on the [Strikethrough \(Del\)](#) icon in the Annotations section.



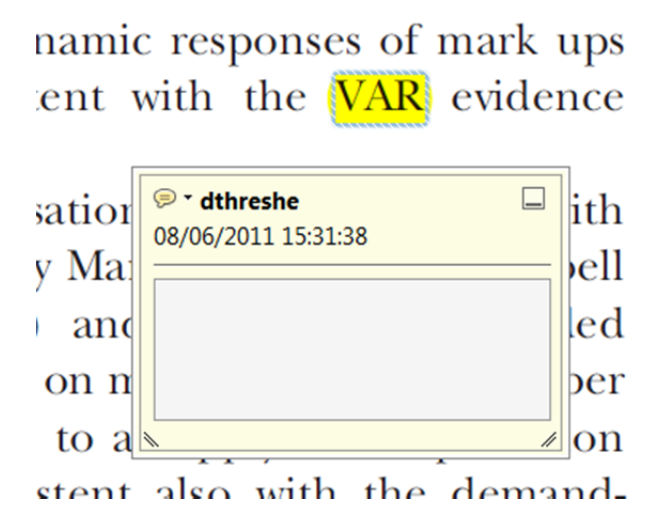
3. [Add note to text](#) Tool – for highlighting a section to be changed to bold or italic.



Highlights text in yellow and opens up a text box where comments can be entered.

How to use it

- Highlight the relevant section of text.
- Click on the [Add note to text](#) icon in the Annotations section.
- Type instruction on what should be changed regarding the text into the yellow box that appears.



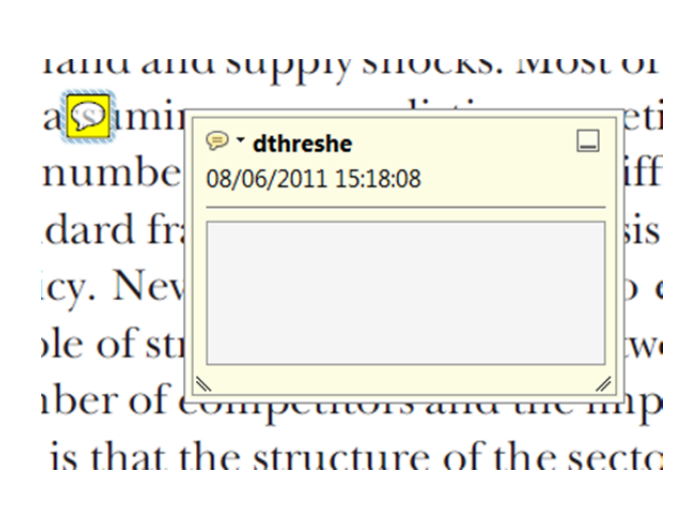
4. [Add sticky note](#) Tool – for making notes at specific points in the text.



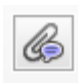
Marks a point in the proof where a comment needs to be highlighted.

How to use it

- Click on the [Add sticky note](#) icon in the Annotations section.
- Click at the point in the proof where the comment should be inserted.
- Type the comment into the yellow box that appears.

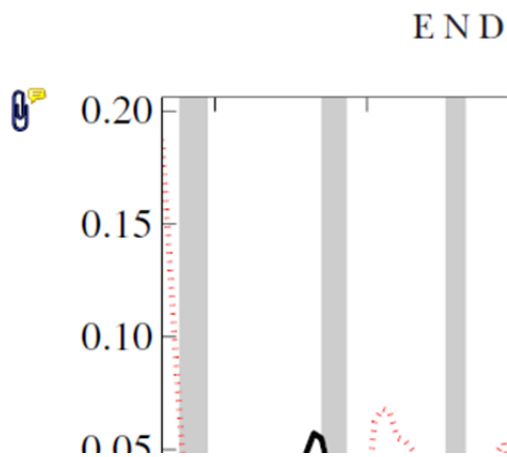


5. **Attach File** Tool – for inserting large amounts of text or replacement figures.


 Inserts an icon linking to the attached file in the appropriate place in the text.

How to use it

- Click on the **Attach File** icon in the Annotations section.
- Click on the proof to where you'd like the attached file to be linked.
- Select the file to be attached from your computer or network.
- Select the colour and type of icon that will appear in the proof. Click OK.



6. **Add stamp** Tool – for approving a proof if no corrections are required.

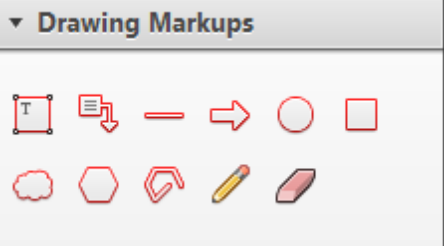
 Inserts a selected stamp onto an appropriate place in the proof.

How to use it

- Click on the **Add stamp** icon in the Annotations section.
- Select the stamp you want to use. (The **Approved** stamp is usually available directly in the menu that appears).
- Click on the proof where you'd like the stamp to appear. (Where a proof is to be approved as it is, this would normally be on the first page).

of the business cycle, starting with the
on perfect competition, constant returns
production. In this environment goods
extra profits and the structure of market
he number of firms in the individual firm
etermined by the model. The New-Key
otaki (1987), has introduced product
general equilibrium models with nominal
ed and supply shocks. Most of this literat

APPROVED

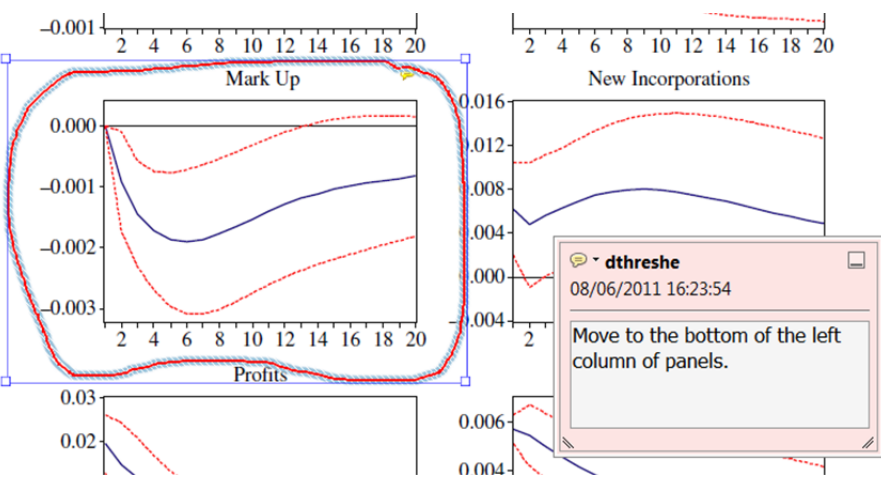


7. **Drawing Markups** Tools – for drawing shapes, lines and freeform annotations on proofs and commenting on these marks.

Allows shapes, lines and freeform annotations to be drawn on proofs and for comment to be made on these marks..

How to use it

- Click on one of the shapes in the **Drawing Markups** section.
- Click on the proof at the relevant point and draw the selected shape with the cursor.
- To add a comment to the drawn shape, move the cursor over the shape until an arrowhead appears.
- Double click on the shape and type any text in the red box that appears.



For further information on how to annotate proofs, click on the **Help** menu to reveal a list of further options:

